New cyclometalated iridium(III) dye chromophore complexes for p-type dye-sensitised solar cells

Alessandro Sinopoli,[a] Christopher J. Wood,[b] Elizabeth A. Gibson*[b] and Paul I. P. Elliott*[a]

[a] Department of Chemistry, University of Huddersfield, Queensgate, Huddersfield, HD1 3DH, UK

[b] School of Chemistry, Newcastle University, Newcastle, NE1 7RU, UK

* Corresponding authors: elizabeth.gibson@ncl.ac.uk; p.i.elliott@hud.ac.uk

Abstract

The synthesis of seven iridium complexes $[Ir(C\hat{}N)_2(N\hat{}N)][PF_6]$ (**AS9-15**) designed as dyes for p-type DSSC is described. These complexes comprise a 4-(pyrid-2-yl)benzoic acid as the cyclometalating/anchoring ligand with different diimine ligands acting as electron accepting ancillary ligands. DFT analysis together with photophysical investigations reveal how using different π-systems on the ancillary ligand it is possible to tune the absorption spectra of these complexes and to enhance the spatial separation between the HOMO and LUMO. Computational studies demonstrate an ideal HOMO to LUMO charge transfer directionality for the presented $[Ir(C\hat{}N)_2(N\hat{}N)]^+$ frameworks, promoting a favourable hole transfer into the NiO cathode valence band upon photoexcitation in p-type DSSC devices. Preliminary tests on NiO-based p-type DSSCs have been carried out confirming the potential use of complexes **AS9-15** as a basis for continued development as DSSC chromophores.

Introduction

There is currently a growing interest in the development of dye-sensitized solar cells (DSSCs) based on p-type inorganic semiconductors (p-SCs) such as nickel oxide (Figure 1). [1] This type of solar cell is based on hole injection into the valence band of the p-SC from the photoexcited sensitiser. Accordingly, the specific electronic properties of the ideal sensitiser for p-SCs significantly differ from those designed for classical Grätzel cells based on the sensitization of a n-type semiconductor (n-SC) such as titanium dioxide. In the latter case, the dye must be a strong reducing agent in its excited-state in order to inject an electron in the conduction band of the n-SC. [2, 3] The electronic requirements of the sensitisers for p-SCs are just the opposite of those for n-SC. In

addition, the sensitisers must be functionalized with anchoring groups, first to firmly graft them on the semiconductor surface and second to provide significant electronic coupling with the semiconductor wavefunction in order to ensure an efficient charge tunnelling from the sensitiser excited-state into the semiconductor.[4, 5] For hole injection into a p-SC, the electron coupling is optimized when the highest occupied molecular orbital (HOMO) of the dye significantly extends over the anchoring groups in order to overlap with the valence band (VB) of the semiconductor. On the other hand, to minimize the charge recombination, the region of the molecule where the LUMO resides, should be kept away from the NiO surface.

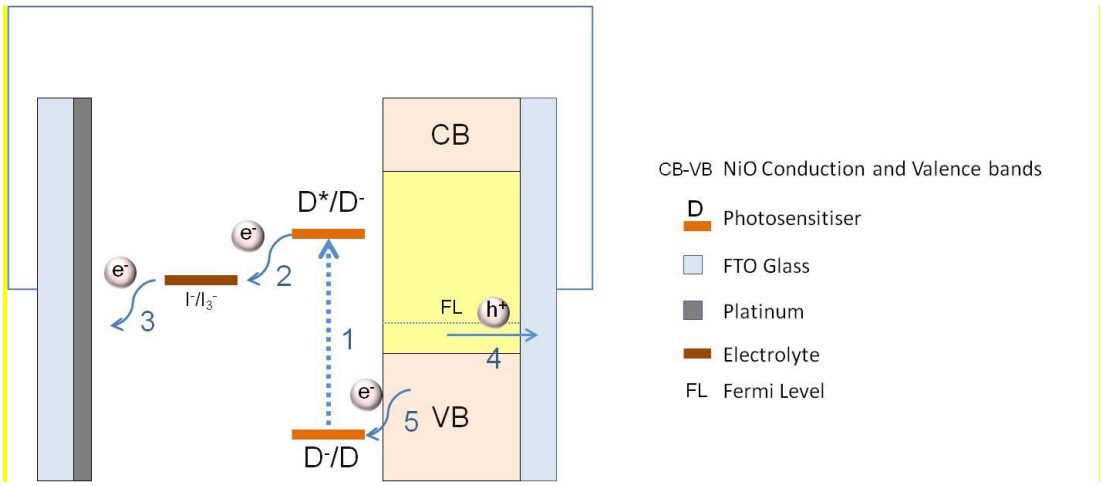

Figure 1. Main operating principles of a p-type dye-sensitised solar cell. D, D^-, D* represent the photosensitiser in the ground, and the reduced and excited states, respectively.(1) photon absorption, (2) reduced dye regeneration, (3) regeneration of the electrolyte, (4) hole injection into NiO valence band, (5) electron transfer to the dye.

The attention toward the development of NiO p-type DSSCs has increased thanks to their potential use in tandem DSSC, involving the combination of a sensitised photocathode with a sensitised photoanode for which, ideally, their absorption should be complementary. Although improvements have been made, [6-8] tandem and p-type cells are plagued with low efficiency values, partly due to rapid (ps timescale [9]) recombination of the photocathode semiconductor hole with the reduced dye.[6] In order to overcome this fundamental obstacle in the tandem and p-type system, work has been focused on increasing the lifetime of both the reduced dye and charge in the semiconductor, designing chromophores that localize the electron farther away from the semiconductor

surface.[8, 10-12]

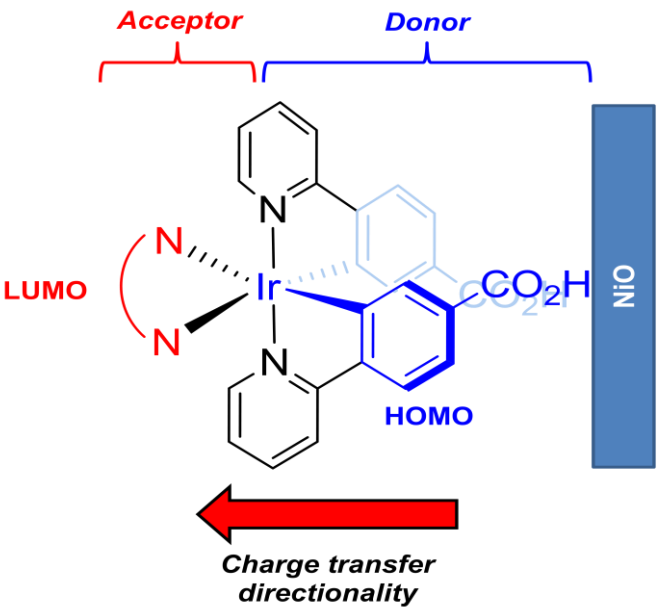

Figure 1. Main design of complexes **AS9-15**, donor fragment (blue), acceptor fragment (red).

Significantly longer charge separation can be achieved in dyes with charge transfer (CT) character, the longest being with weakly coupled, separate donor and acceptor units. The latter have been long-lived enough to allow the use of redox couples other than I_3^-/I^-,[13, 14] most notably cobalt polypyridine complexes that also have recently given breakthrough results in TiO_2 DSSCs [15, 16] and could then allow extension to p-type or tandem cells with Co(III/II) electrolytes. [17]

Iridium bis cyclometalated hetereleptic complexes are interesting in this regard as they have intrinsic CT excited state character. The main advantages include the fact that isomers are not a problem as synthesis is regioselective which makes CT directionality highly predictable, they also offer photophysical and electronic tunability of the ligands for further optimization. The iridium wide colour tunability and high phosphorescence quantum yield, [18, 19] make it very attractive for luminescent application as organic light-emitting diodes (OLEDs), [20-23] phosphorent materials, [24, 25] and, more recently, anticancer agents, [26-28] generating an explosion of new cyclometalated iridium(III) complexes reported in the last decade. [29] Iridium based photosensitisers have recently been reported for p-type DSSCs, but with modest results.[30, 31] Moreover, the majority of dyes tested with n- and p-type semiconductors are anchored through carboxylic acid groups attached on an ancillary ligand

[1, 7, 8, 32] which is not necessarily optimal for hole injection since being e^- withdrawing they generally favour localisation of the lowest unoccupied molecular orbital (LUMO) on these ligands. [4, 5]

The design of a p-type dye reported here (Figure 1) comes mainly from the need to prevent the recombination of the injected hole with the excited electron together with a reasonable absorption of the visible light. The carboxylate anchoring groups are placed on the electron donating anionic aryl groups. This should maintain efficient anchoring onto the electrode but ensure localization of the HOMO on these moieties. Use of a neutral electron accepting ancillary ligand *trans* to the anchoring arylcarboxylate rings thus ensures localization of the LUMO away from the anchoring groups thereby maximising charge separation and minimising recombination. Examples of this Ir(pybaH)$_2$(N^N) type architecture have been previously reported with applications in MOF oxygen sensors, luminogenic probes and ion probes but have not been applied as DSSC chromophores. [33-35] This electron donor moiety is then combined with neutral electron accepting ligands (Figure 2). These range from the simple and ubiquitous bipyridine and phenanthroline (**AS9** and **AS10**) to more electronwithdrawing ligands such as dipyrido[3,2-a:20-30-c]-phenazine (dppz) (**AS11**) [36] as well as nitro-substituted bpy ligands (**AS12** and **AS13**) to red shift the absorption spectra.[37] We have also included in this series BIAN-type [bis(arylimino)acenaphthene] ligands known to yield panchromatic absorption in their Ir(III) cyclometalated complexes (**AS14** and **AS15**). [38]

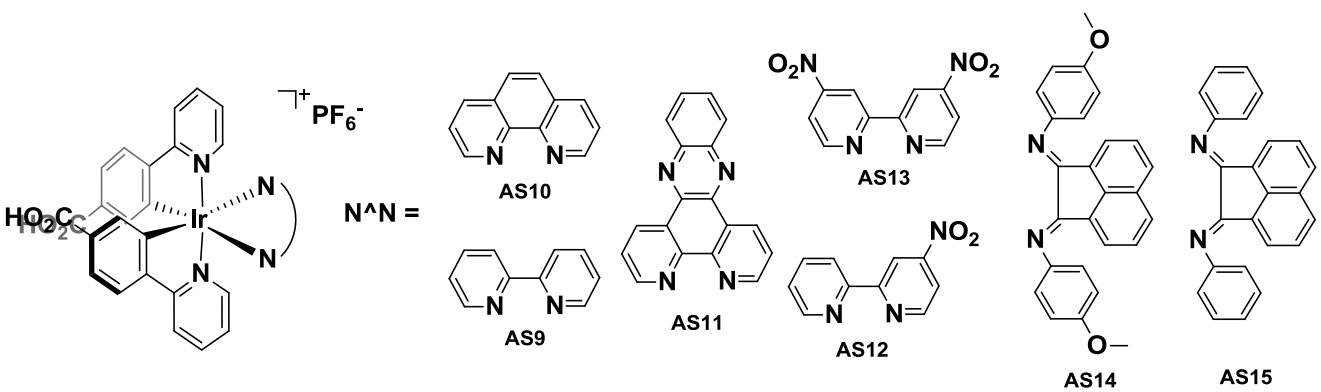

Figure 2. Iridium biscyclometalated complexes prepared (**AS9-15)**. Ancillary ligands used for p-type complexes synthesis (N^N): (**AS9**) bipyridine; (**AS10**) phenanthroline; (**AS11**) dipyrido[3,2-a:20-30-c]-phenazine; (**AS12**)

4-nitrobipyridine; (**AS13**) 4,4'-dinitrobipyridine; (**AS14**) N,N'-bis(4-methoxyphenylimino)acenaphthene; (**AS15**) N,N'-bis(phenylimino)acenaphthene.

Results & Discussion

The cyclometalating ligand precursor designed for the reported p-type dyes, has been prepared by oxidizing the tolylpyridine to pyridylbenzoic acid (pybaH) with $KMnO_4$. The cyclometalated complexes **AS9-15** were prepared using a two-step procedure that is depicted in Scheme 1. [39] Iridium (III) chloride and the 4-(2-pyridyl)benzoic acid ligand were combined in ethoxyethanol/water (3:1) and heated to reflux.

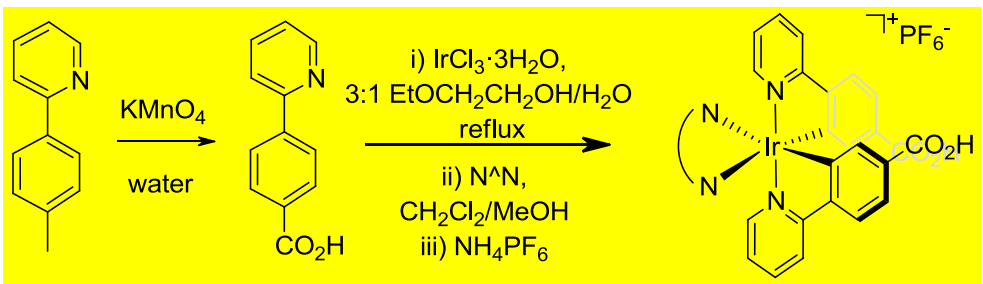

Scheme 1. Synthetic route of complexes **AS9-15.**

The reaction mixtures are observed to change from dark red to bright orange within 15 to 30 minutes once the reaction reaches the point of reflux. To ensure complete consumption of the metal salt, the reactions were heated for four hours and then allowed to cool to room temperature. The crude dimer solution $[Ir(pyba)_2Cl]_2$ was reduced under vacuum to a minimal volume and recrystallised from dichlormethane/hexane, collected by filtration and was used without further purification or characterisation. The dimer was then reacted with the corresponding ancillary ligand in refluxing dichloromethane/methanol. The product was purified by column chromatography on silica and the resulting solids were dissolved in a minimum volume of methanol and NH_4PF_6 was added. The products were recrystallised by addition of diethyl ether to yield from yellow to dark red solids in modest yields. The complexes $[Ir(pyba)_2(N^N)]PF_6$, **AS9-15**, were then fully characterised using ^1H and ^{13}C NMR spectroscopy and mass spectrometry.

The cyclometalation of pyba ligand is evidenced by ^{1}H NMR spectroscopy whereby the corresponding complexes show the loss of one proton in the aryl fragment together with a shift to higher field by ~ 0.5 ppm for the signals corresponding to the protons adjacent to the coordinated carbon and to the coordinated nitrogen.

In the ^{1}H NMR spectra, **AS9-12** and **AS14-15** complexes show a single set of resonances for the two cyclometalated ligands as consequence of the C_2 symmetry of the complexes. The peaks distribution for the coordinated diamine ligands shows that half of the ligand is in an unique NMR environment, further reflecting this symmetry. Complex **AS13** is the only asymmetric complex due to the unsymmetrical NO_2-bpy ligand, for this reason all its protons exhibit unique resonances.

UV-Visible absorption spectra were recorded for all complexes in aerated acetonitrile solutions at room temperature and are presented in Figure 3 with data summarised in Table 1. The absorption spectra of these compounds show intense bands in the ultraviolet region between 250 and 350 nm (Figure 3). These bands are attributed to spin-allowed π-π* ligand-centred (^{1}LC) transitions. These assignments were made on assessment of closely related metal complexes in the literature.[40, 41] The less intense, lower energy absorption features from 350 to 500 nm are due to ^{1}MLCT/^{1}LLCT charge-transfer (CT) transitions. Two types of CT transitions can be distinguished in the spectra: bands of moderate intensity between 350 and ~450 nm, assigned to ^{1}MLCT/^{1}LLCT transitions, and transitions with weaker intensity (~ 450 – 550 nm), tentatively assigned as being spin forbidden ^{3}MLCT in character. [42]

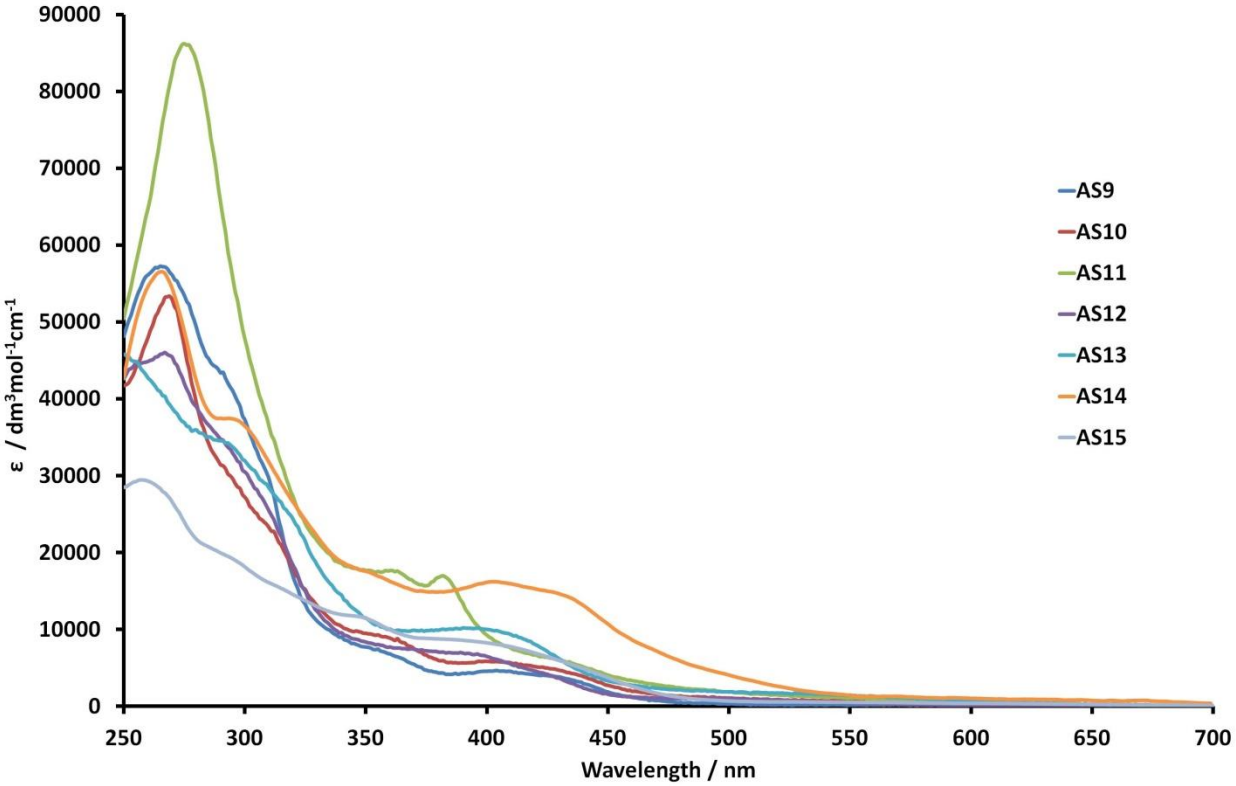

Figure 3. Absorption spectra of **AS9-15** dyes in acetonitrile.

AS9 and **AS10** have very similar absorption profiles and their absorptions in the visible region is limited to a weak band (ε_{410nm} ≈4200 $M^{-1}\cdot cm^{-1}$) about 410 nm. The absorption profile of **AS11** is dominated by a strong transition at 274 nm (^{1}LC dppz centred) plus a structured ^{1}MLCT band at 433 nm. Complexes **AS12** and **AS13** have similar profile and, as expected, the presence of two nitro groups for **AS13** helps to enhance the absorption, (ε_{390nm} ≈10000 $M^{-1}\cdot cm^{-1}$ for **AS13** *vs* 6800 $M^{-1}\cdot cm^{-1}$ for **AS12**). Complex **AS14** has clearly the strongest absorption in the visible range within the complexes presented in this work with a strong band across 430 nm followed by a tail beyond 550 nm. BIAN based ligands have been used previously by Zysman-Colman *et al.* [38] to yield panchromatic absorbing complexes, able to shift the absorption of the complex into the red and near-IR region. The absorption profile of complex **AS15** is clearly affected by the absence of the MeO groups on the phenyl rings, in agreement with the results showed by Zysman-Colman *et al* [38], hence the complex absorption profile does not as extensive and is not as intense (ε_{401nm} ≈8100 $M^{-1}\cdot cm^{-1}$) as that for **AS14**.

Table 1. Summarised photophysical absorption and emission data for complexes **AS9-15** in aerated acetonitrile.

Dye	λ_{max}^{abs}/ nm (ε / $dm^3\,mol^{-1}\,cm^{-1}$)	λ_{max}^{em}/ nm	τ / ns
AS9	265 (57200), 289 (43400), 356 (7933), 417 (4250)	508, 535	146
AS10	267 (53300), 306 (24300), 354 (7390), 405 (4600)	505, 536	144
AS11	274 (86202), 362 (17538), 381 (16936), 433 (5380)	-	-
AS12	267 (46014), 302 (28981), 391 (6871)	-	-
AS13	253 (47529), 291 (34300), 390 (10000)	-	-
AS14	265 (56517), 295 (37402), 402 (16210), 431 (14514)	-	-
AS15	256 (29463), 295 (19024), 347 (11653), 401 (8139)	-	-

Normalised emission spectra are presented in Figure 4. Complexes **AS9** and **AS10** exhibit intense structured emission bands, with vibronic progression, with maxima at 508 nm and 535 nm which is characteristic of phosphorescent emission from ^{3}MLCT/^{3}ILCT states, dominated by the [Ir(pyba)$_2$] fragment. [33, 40] Luminescence lifetimes were also determined in aerated acetonitrile with a value of *ca* 145 ns for both **AS9** and **AS10**, consistent with phosphorescent emission from a triplet state. The carboxylic acid EWGs, placed on the pyba ligands, bring down in energy the pyba unoccupied orbitals compared to those of ppy, such that the excited electron in the emissive excited state must be localised on the pyridyl rings of the pyba instead of the ancillary bpy as is the case for [Ir(ppy)$_2$(bpy)]$^+$ which exhibits ^{3}MLCT/^{3}LLCT-based emission at 591 nm. [43] All the other complexes are essentially non-emissive and here we expect that the greater electron-withdrawing character of the ancillary ligands results in ^{3}MLCT/^{3}LLCT states which must decay non-radiatively to the ground state.

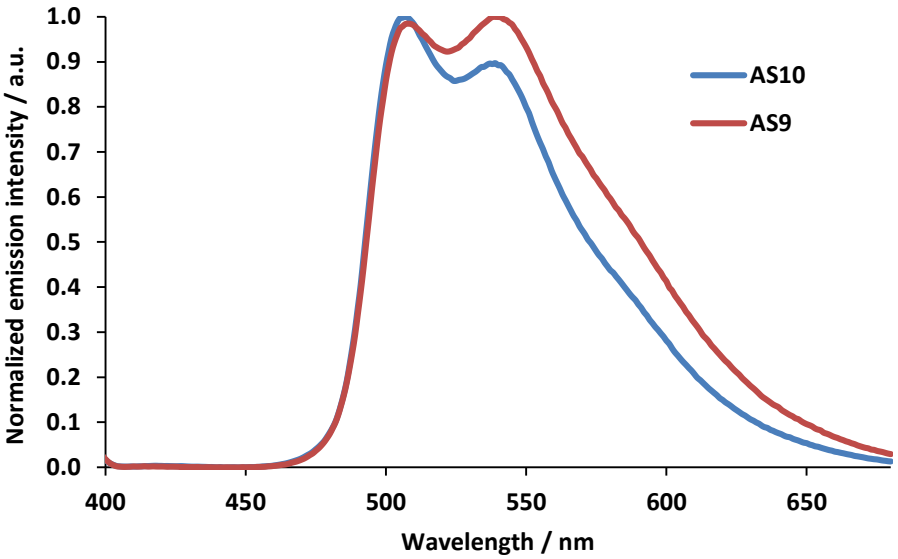

Figure 4. Normalised emission spectra for complexes **AS9-10** in aerated acetonitrile at RT (λ^{ex} = 365 nm).

Electrochemical analysis was complicated by limited solubility of the dyes and therefore did not yield satisfying informative results. Some reversible or quasi reversible oxidation waves for **AS9-14**, corresponding to the one-electron Ir^{III}/Ir^{IV} couple could be observed, however, occurring in the range between +1.02 and +1.19 V (*vs* Fc/Fc^{+}) consistent with the expectation of delocalization of the HOMO on the cyclometalating fragment.

To aid in our understanding of the photophysical properties of the complexes prepared we carried out gas-phase density functional theory (DFT) calculations. The orbital analysis reveals the spatial distribution of the HOMO and LUMO are perfectly set to promote charge transfer directionality away from the NiO surface and minimize the recombination. The HOMO localised on the anchoring ligand, as expected, makes the electronic distribution on these complexes ideal for their hole injection into the nickel oxide electrode when incorporated in a DSSC device.

Looking at the orbital distribution on complex **AS11**, it is interesting to note that for the dppz ligand the LUMO is localised on the pyrazine rather than on the bpy-like part of the ligand, as previously reported in literature for similar dppz complexes, which should lead to increased charge separation.[36] In complexes **AS12-13**, the LUMO is delocalised on the dinitro-bpy for **AS13** and on the nitro-pyridine fragment for **AS12**, as consequence of its

asymmetry. The computational data obtained for complexes **AS14** and **AS15** are in line with those reported by Zysman-Colman *et al.* [38, 44] for $[Ir(ppy)_2(BIAN)][PF_6]$ and $[Ir(ppy)_2(MeOBIAN)][PF_6]$. In particular the LUMO is localized on the BIAN fragment and the HOMO on the pyba ligands.

Despite the emissive state for **AS9-10** being ^{3}MLCT/^{3}ILCT in character, the ground state LUMO for these complexes is also on the diimine ligand. However, the order of excited states doesn't necessarily follow the order of the ground state orbitals associated with them, when their respective unoccupied orbitals are brought into close energetic proximity.

The energy levels of the frontier orbitals are shown in Figure 5 and the corresponding HOMO-LUMO energies are reported in Table 2. The calculated HOMO energies remain relatively unchanged as would be expected for the consistency of the pyba ligand across the series with a value of about -6.2 eV. However, the introduction of electron withdrawing nitro substituents on the bipyridyl skeleton in **AS12-13**, leads to a significant stabilization of the LUMO relative to those of complexes **AS9** and **AS10** by more than 1 eV. For complexes **AS14** and **AS15**, the BIAN fragment brings down in energy the LUMO, compared to the bpy analogue, by approximately 0.7 eV.

Table 2 HOMO, LUMO and HOMO-LUMO gap energy values for complexes **AS9-15**

Dye	HOMO / eV	LUMO / eV	Δ / eV
AS9	-6.04	-2.63	3.41
AS10	-6.05	-2.65	3.40
AS11	-6.07	-3.09	2.98
AS12	-6.16	-3.66	2.50
AS13	-6.26	-3.90	2.36
AS14	-5.94	-3.30	2.64
AS15	-6.02	-3.39	2.63

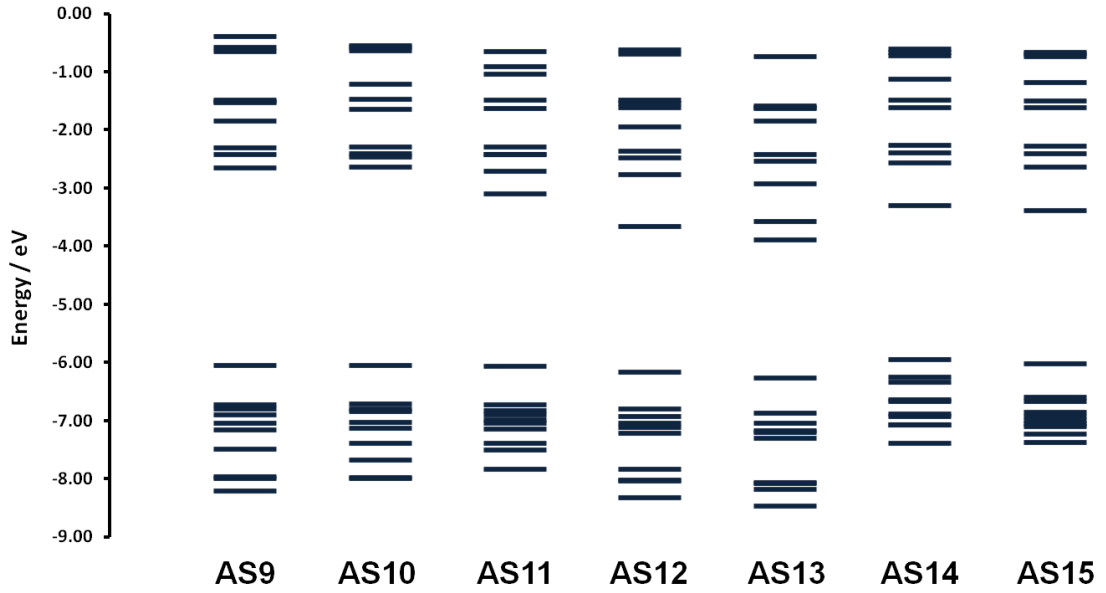

Figure 5. Molecular orbital energy level diagram for complexes **AS9-15**

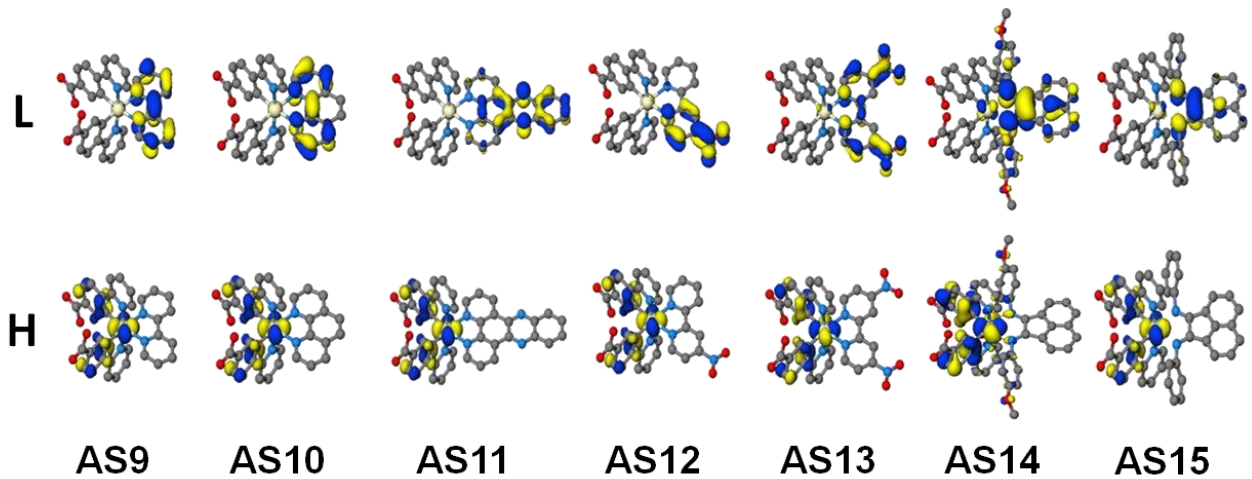

Figure 6. Plots of HOMO (bottom) and LUMO (top) orbitals for complexes **AS9-15**.

Time-dependent DFT (TDDFT) calculations were carried out on the optimised ground state geometries of each complex in order to determine vertical excitation energies. From TDDFT analysis (Figure 7 and ESI), the predicted transitions correlate well with the experimental spectra.

The excitations to the S_1 state all complexes are primarily HOMO→LUMO in character, however, they are of low oscillator strength and will therefore contribute little to the observed absorption spectra. The S_1 transition for complexes **AS9-11** takes place below 500 nm, whereas the S_1 for all the other complexes, occurs beyond 630

nm (see ESI). The major transitions observed for all complexes between 350 and 500 nm are primarily of ^{1}MLCT character (see ESI), with generally charge transfer from Ir/aryl to ancillary ligand. Below 300 nm most of the transitions are ^{1}LC in character, for example **AS11** shows a transition at 283 nm with a high oscillator strength which is ILCT in character with charge transfer from the distal phenazine to the proximal phenantroline moieties of the dppz ligand. Only **AS14** shows a strong transition beyond 450 nm of ^{1}MLCT/^{1}ILCT character, with a substantial contribution of the MeO-BIAN fragment.

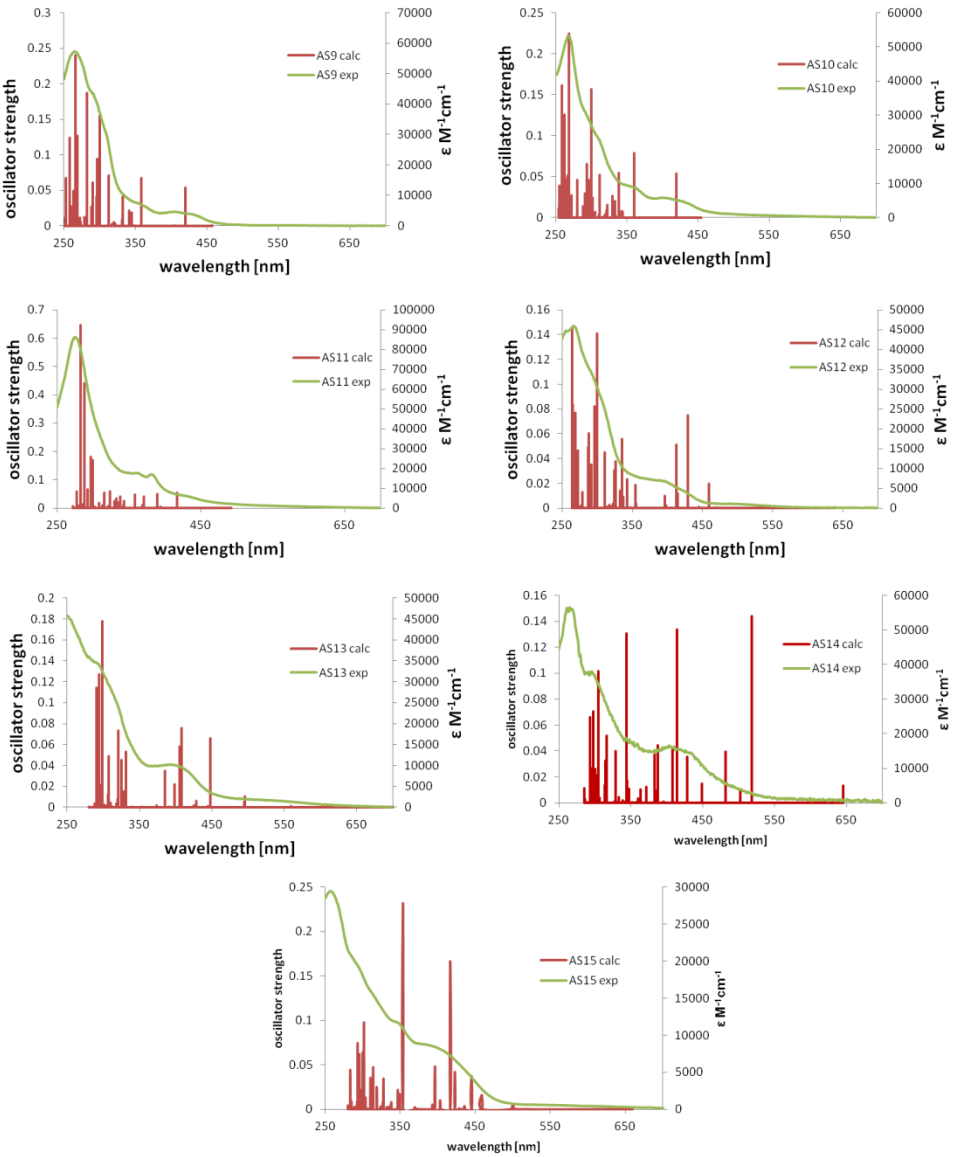

Figure 7. TDDFT calculated transitions for complexes **AS9-15** with experimental spectra overlaid.

The photovoltaic properties of the complexes as dyes in p-type NiO based DSSC were evaluated in preliminary test devices. Complex **AS15** wasn't tested because of its low solubility. The dye coated film was prepared using a water/ethanol solution of $NiCl_2$ and a triblock co-polymer, F108. Platinised fluorine-doped tin oxide (FTO) glass was used as the counter electrode and the electrolyte was a solution of 0.1 M I_2 and 1.0 M LiI in acetonitrile. The cells were thermally sealed before measurements. Photovoltaic measurements were performed on an AM 1.5 solar simulator (100 mW cm^{-2}) and the incident light was calibrated by using a Si photodiode reference. JV curves were obtained by applying an external bias to the cells and measuring the generated photocurrent with a Keithley digital source meter.

Figure 8 reports the IPCE data for complexes **AS9-14**, which all exceed the IPCE for un-dyed NiO ; this suggests they each photosensitise NiO. The IPCE values are between 10 and 25% and their profiles reflect the corresponding absorption spectra of the dyes. Unfortunately the presented dyes have their main absorption bands at or below ~ 500 nm and so the IPCE traces similarly tail off in this region. Only **AS13-14**, which present the highest extinction coefficients in the visible region, generate reasonable IPCE values.

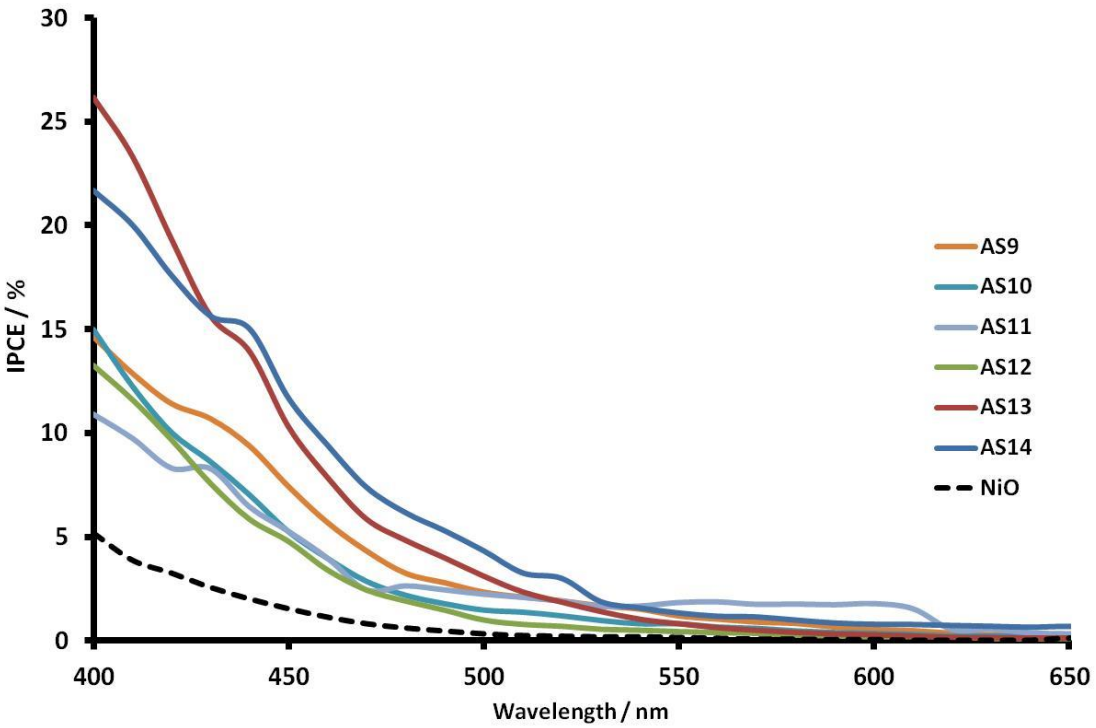

Figure 8. IPCE spectra for p-type cells sensitised using iridium complexes **AS9-14.**

All the applied complexes, under irradiation, were able to generate a photocurrent. The photovoltaic performances of solar cells based on these iridium complexes **AS9-14** are summarised in Table 3. Figure 9 shows the current–voltage characteristics of the dyes under AM 1.5. Both IPCE and efficiency values for **AS11** and **AS12** may have been affected by their low solubility as a dilute dye solution presumably limits the dye loading on the immersed electrodes. As expected from their very similar structures, **AS9** and **AS10** showed nearly identical results in terms of IPCE and efficiency. Complex **AS13** showed better performances in terms of both IPCE value and efficiency compared to the mono-nitro bpy based **AS12**, this can be attributed to the presence of two electronwithdrawing nitro groups on **AS13** able to stabilise the LUMO, narrowing the HOMO-LUMO gap, extending the complex absorption more in the visible region. Complexes **AS13** and **AS14** showed the best efficiencies of 0.032% and 0.043% respectively, attributable to their enhanced absorption in the visible spectrum compared to the rest of the series. The reported efficiencies seem to follow the trend of IPCE intensities shown in Figure 8.

Table 3. Photovoltaic parameters of tested dyes.

Dye	J_{sc} / mA cm^{-2}	V_{oc} / V	FF / %	η / %
AS9	0.68	0.09	36.6	0.022
AS10	0.66	0.09	37.6	0.022
AS11	0.45	0.07	38.1	0.013
AS12	0.36	0.09	40.1	0.013
AS13	0.82	0.10	38.7	0.032
AS14	1.12	0.10	36.8	0.043

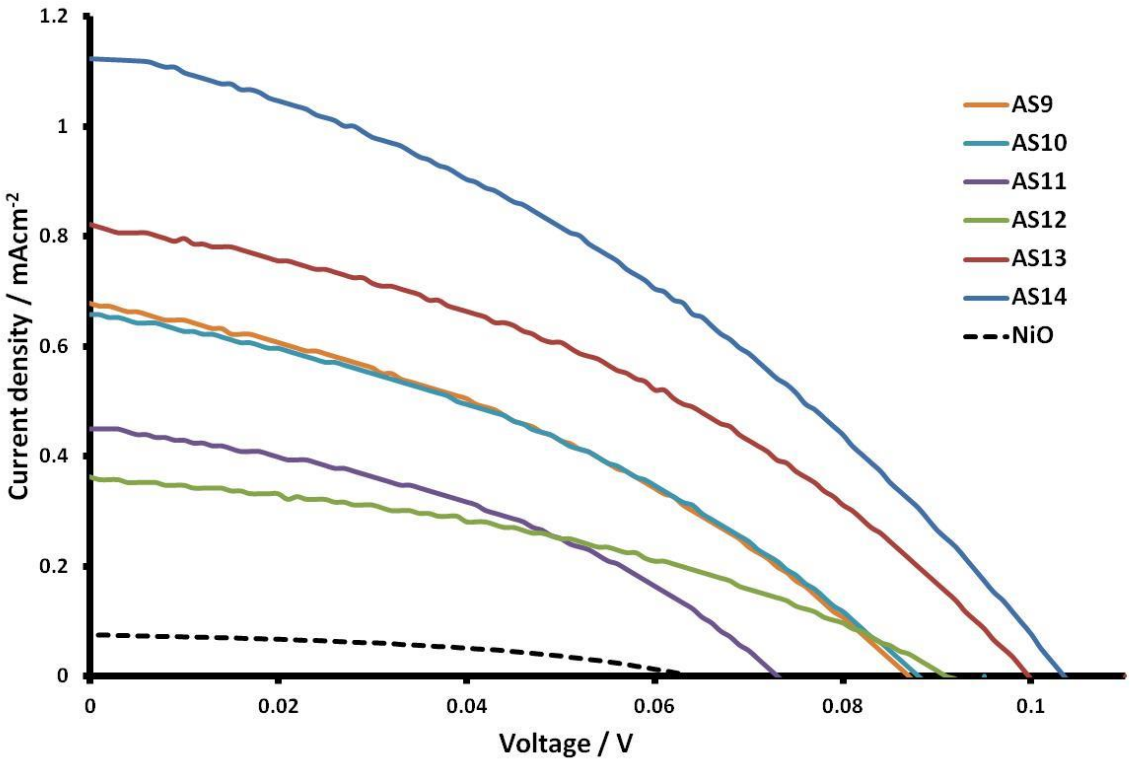

Figure 9. Current-Voltage curves DSSC constructed using iridium complexes **AS9-14.**

Conclusions

We have prepared and characterised, by ^{1}H and ^{13}C NMR spectroscopy, mass spectrometry and investigated the photophysics by UV-Visible absorption and emission spectroscopy, seven new iridium(III) dyes with various ancillary ligands. Computational calculations were fundamental tools in the theoretical characterisation of the new complexes and in the prediction and explanation of their proprieties. Diimine complexes show good tuning of absorption wavelengths and HOMO-LUMO gap, and thanks to their design, these complexes show spatial charge transfer directionality together with energy levels in accordance with their intended application in p-DSSC. The use of these complexes as sensitisers in DSSC devices has been investigated. All tested complexes achieved modest efficiencies with **AS13** and **AS14** showing the best efficiencies of 0.032% and 0.043% respectively. these are nevertheless encouraging results when related to the 0.068% efficiency reported for $[Ir(ppy)_2(N\text{^}N)]^+$ -based complexes, bearing methyl phosphonic acid as anchoring groups, by Gennari *et al.* [30] and to the 0.020% previously reported by our group, using the coumarin C6 complex $[Ir(C6)_2(dcb)]^+$.[31] The methodology reported here will allow for facile tuning of photophysical and photovoltaic properties and produce

dyes with greater ease than existing ruthenium based systems. Results are encouraging for the development of a new generation of p-type dyes based on this general design. Future research will focus on improving on these initial studies and increasing the light absorbing properties of these dyes together with the substitution of the triiodide/iodide electrolyte for a one-electron, outer sphere redox couple such as cobalt polypyridyl complexes, in order to relieve the constraint that the complexities of the iodine-based system impose on the energetic requirements of the dye. [45]

Acknowledgements

The authors thank the University of Huddersfield for funding this research. Through membership of the UK Materials Chemistry Consortium (EPSRC grant no EP/L000202) also acknowledges the ARCHER UK National Supercomputing Service (http://www.archer.ac.uk) as well as the University of Huddersfield High Performance Computing Research Group for computational resource utilised in this work.

Materials and general synthetic procedures

Chemicals were purchased from Aldrich and Acros, iridium was purchased from Precious Metals Online (Australia) and used as received. All complexation reactions were carried out under nitrogen. Dppz dipyrido[3,2-a:20-30-c]-phenazine [46], 4-nitro-bipyridine and 4,4'-dinitro-bipyridine [47, 48], BIAN [bis(arylimino)acenaphthene] [49] were prepared according to literature methods.

All the compounds prepared in this work were characterized by ^{1}H NMR and ^{13}C NMR spectrometry; spectra were obtained on a Bruker Advance 400 MHz instrument. Mass spectrometry data were collected on a Bruker MicroTOF-Q instrument and Agilent 6210 TOF MS. UV-Visible absorption spectra were recorded on an Agilent Cary 60 UV-Vis spectrophotometer and corrected emission spectra were recorded on a Horiba Fluoromax-4 Spectrofluorometer. Luminescent lifetime measurements were carried out using an Edinburgh Instruments Mini-Tau spectrometer.

Dye sensitised solar cell fabrication

NiO electrodes were made by applying the precursor solution described in previous literature [50] onto conducting glass substrates (Pilkington TEC15, sheet resistance 15 Ω/sq) by doctor blade using adhesive tape (3M) as spacer (0.2 cm^2 active area), followed by sintering in a NaberthermB150 oven at 450 °C for 30 min. NiO films

were immersed in dye solutions (0.3 mM) for 12 h. The dyed NiO electrode was assembled face-to-face with a platinised counter electrode (Pilkington TEC8, sheet resistance 8 Ω/sq) using a 30 μm thick thermoplastic frame (Surlyn 1702). The electrolyte, containing LiI (1.0 M) and I_2 (0.1 M) in acetonitrile, was introduced through the predrilled hole in the counter electrode, which was sealed afterward. The active area was 0.25 cm^2.

Computational methods

DFT calculations were carried out using the NWChem 6.3 software package [51]. Calculations were carried out using the B3LYP hybrid functional (20% Hartree–Fock), [52] Stuttgart relativistic small core ECP [53] for transition metals and 6-311G* basis sets [54] for all other atoms. Molecular structures and molecular orbitals were visualized using the ccp1 graphical user interface. The ground state geometries of all complexes were first optimized and molecular orbital energies determined. TDDFT calculations were then used at the ground state geometries to derive vertical excitation energies and hence simulated absorption spectra. TDDFT calculations on optimised structures in CH_3CN by using the COSMO solvation model, [55] built in NWChem software, were used to obtain the electronic spectra and molecular orbital energy levels.

Synthesis of 4-(2-pyridyl)benzoic acid (pyba)

This synthetic procedure was adapted from ref [56]. Tolyl-pyridine was oxidized with $KMnO_4$ as follows: a mixture of tolyl-pyridine (0.514 g) and $KMnO_4$ (1.54 g) in water 50 mL was heated at 70°C for 24 h. After filtration of the reaction mixture and washing the filtrate with aqueous NaOH (1M, 5 mL), the combined water fraction were collected and washed three times with $CHCl_3$ to remove unconverted starting material. The aqueous solution was neutralized with HCl (1M) and concentrated (30 mL). After acidifying to pH 4, the precipitate was collected, washed with ethanol and dried in vacuum yielding a white powder. (Yield 85%)

^{1}H NMR (400 MHz, CD_3OD) δ:8.57 (d, ^3J = 4.46, 1H, Py-*H*); 8.05 (d, ^3J = 8.23, 2H, Ar-*H*); 7.97 (d, ^3J = 8.23, 2H, Ar-*H*); 7.87 (d, ^3J = 3.43, 1H, Py-*H*); 7.37-7.33 (m, 2H, Py-*H*).

^{13}C {^{1}H} NMR (400 MHz, DMSO-d_6): 168.04, 154.59, 148.75, 141.78, 139.90, 131.51, 130.44, 129.98, 127.55, 124.50, 122.69.

HRMS (ESI) *m/z* calcd 199.0633 for $C_{12}H_9NO_2$, found 200.0706 $(M+H)^+$

Synthesis of [Ir(4-(2-pyridyl)benzoic acid)$_2$Cl]$_2$

353 mg of $IrCl_3 \cdot 3H_2O$ (1 mmol) were dissolved in 35 mL 2-ethoxyethanol:water 3:1 in 2 necked round bottom flask and degassed with N_2 at 80°C for 20 minutes. 2 equivalents (400 mg) of 4-(2-pyridyl)benzoic acid were added and heated to reflux temperature for 4 hours. The solution was reduced to a minimal volume and recrystallized from DCM/Hexane. The dimer was used without any further characterization or purification.

Synthesis of [Ir(pyba)$_2$(2,2'-bipyridine)]PF$_6$ (AS9)

2,2'-bipyridine (0.025 g, 0.16 mmol) was dissolved in DCM:MeOH 2:1 (6 mL) and $[Ir(pyba)_2(Cl)]_2$ (0.100 g, 0.08 mmol) was added. The mixture was heated at reflux under nitrogen atmosphere, in the dark. After 6 hrs, the yellow solution was cooled to room temperature. The crude solid was purified by column on silica eluted with MeCN:H_2O:KNO_3 7:1:0.5. The yellow fraction was dried under vacuum, redissolved in acetonitrile and filtered. The solution was dried again and the solid was dissolved in a minimal amount of methanol and NH_4PF_6 (130 mg, 0.9 mmol) was added allowed to stir overnight. The solution was left in the fridge for two hours, recrystallised with ether and then filtered on sintered glass. A yellow powder was collected by filtration. (42 mg, yield 30%)

^{1}H NMR (400 MHz, CD_3CN) δ:8.55 (d, ^{3}J = 8.36, 2H, Bpy-*H*); 8.20 (d, ^{3}J = 8.36, 2H, Pyba-*H*); 8.16 (t, ^{3}J = 6.18, 2H, Bpy-*H*); 8.00-7.94 (m, 4H, Bpy-*H*&Pyba-*H*); 7.93 (d, ^{3}J = 8.36, 2H, Pyba-*H*); 7.71-7.67 (m, 4H, Pyba-*H*); 7.51 (t, ^{3}J = 6.84, 2H, Bpy-*H*); 7.17 (t, ^{3}J = 6.59, 2H, Pyba-*H*); 6.89 (s, 2H, Pyba-*H*).

^{13}C {^{1}H} NMR (400 MHz, CD_3CN): 167.15, 166.58, 156.29, 151.48, 150.21, 149.79, 149.29, 140.14, 139.61, 132.63, 131.29, 129.10, 125.32, 125.30, 125.26, 124.85, 121.70.

MS (ESI) *m/z* calcd for $[C_{34}H_{24}IrN_4O_4]^+$ 745.1426, found 745.1427 (M^+).

Synthesis of $[Ir(pyba)_2(1,10\text{-phenanthroline})]PF_6$ (AS10)

The synthetic procedure was the same as that for **AS9**, except that 1,10-phenanthroline (0.027 g, 0.16 mmol), which replaced 2,2'-bipyridine, was used. The resulting product was purified and precipitated as for **AS9**, yielding a bright yellow powder. (20 mg, yield 13%)

^{1}H NMR (400 MHz, CD_3CN) δ:8.72 (dd, ^3J = 8.23, ^4J = 1.27, 2H, Phen-*H*); 8.31 (dd, ^3J = 8.5, ^4J = 1.27, 2H, Phen-*H*); 8.26 (s, 2H, Phen-*H*); 8.19 (d, ^3J = 8.00, 2H, Pyba-*H*); 7.96 (d, ^3J = 8.23, 2H, Pyba-*H*); 7.90 (td, ^3J = 7.30, ^4J = 1.51, 2H, Phen-*H*); 7.86 (dd, ^3J = 8.24, ^4J = 5.03, 2H, Phen-*H*); 7.72 (dd, ^3J = 8.23, ^4J = 1.62, 2H, Pyba-*H*); 7.51 (dd, ^3J = 5.45, ^4J = 0.70, 2H, Pyba-*H*); 7.00 (td, ^3J = 5.33, ^4J = 1.27, 4H, Pyba-*H*)

^{13}C {^{1}H} NMR (400 MHz, CD_3CN) δ:166.62, 152.12, 150.38, 149.55, 149.29, 147.27, 139.50, 139.31, 132.83, 132.23, 128.86, 127.98, 127.41, 126.65, 125.21, 125.15, 124.92, 121.6.

MS (ESI) *m/z* calcd for $[C_{36}H_{24}IrN_4O_4]^+$ 769.142, found 769.2015 (M^+).

Synthesis of $[Ir(pyba)_2(2,5\text{-bis}(2\text{-pyridyl})\text{pyrazine})]PF_6$ (AS11)

The synthetic procedure was the same as that for **AS9**, except that 2,5-bis(2-pyridyl)pyrazine (0.043 g, 0.154 mmol), which replaced 2,2'-bipyridine, was used. The resulting product was purified and precipitated as for **AS9**, yielding a dark yellow powder. (28 mg, yield 17.8 %)

^{1}H NMR (400 MHz, CD_3CN) δ:9.80 (d, ^3J = 8.22, 2H, Dppz-*H*); 8.51-8.47 (m, 2H, Dppz-*H*); 8.41 (d, ^3J = 4.40, 2H, Dppz-*H*); 8.23 (d, ^3J = 8.03, 2H, Pyba-*H*); 8.18-8.14 (m, 2H, Dppz-*H*); 8.04-7.90 (m, 6H, Dppz-*H*&Pyba-*H*); 7.75 (d, ^3J = 8.22, 2H, Pyba-*H*); 7.71 (d, ^3J = 4.97, 2H, Pyba-*H*); 7.05 (t, ^3J = 6.50, 2H, Pyba-*H*); 7.00 (s, 2H, Pyba-*H*).

[Low solubility] ^{13}C {^{1}H} NMR (400 MHz, CD_3CN): 166.05, 152.80, 150.07, 149.61, 148.92, 148.44, 142.80, 139.93, 139.11, 135.38, 132.57, 132.25, 131.34, 129.65, 128.39, 124.77, 124.67, 124.50, 121.16.

MS (ESI) calcd for $[C_{42}H_{26}IrN_6O_4]^+$ 871.1644, found 871.1631 (M^+).

Synthesis of $[Ir(pyba)_2$(4-nitro-2,2'-bipyridine)$]PF_6$ (AS12)

The synthetic procedure was the same as that for **AS9**, except that 4-nitro-2,2'-bipyridine (0.031 g, 0.16 mmol), which replaced 2,2'-bipyridine, was used. The resulting product was purified and precipitated as for **AS9**, yielding an orange powder. (28.6 mg, yield 20%)

^{1}H NMR (400 MHz, CD_3CN) δ:9.81 (d, ^3J = 1.88, 1H, Bpy-*H*); 8.77 (d, ^3J = 8.15, 1H, Bpy-*H*); 8.28 (d, ^3J = 5.95, 1H, Bpy-*H*); 8.26-8.20 (m, 3H, Bpy-*H*); 8.10 (dd, ^3J = 5.95, ^4J = 1.88, 1H, Bpy-*H*); 8.04 (d, ^3J = 5.33, 1H, Bpy-*H*); 8.01-7.92 (m, 4H, Pyba-*H*); 7.73-7.66 (m, 4H, Pyba-*H*); 7.60 (t, ^3J = 6.42, 1H, Bpy-*H*); 7.18 (t, ^3J = 6.42, 1H, Pyba-*H*); 7.16 (t, ^3J = 6.58, 1H, Pyba-*H*); 6.89 (d, ^3J = 1.10, 1H, Pyba-*H*); 6.85 (d, ^3J = 1.10, 1H, Pyba-*H*).

[Low solubility] ^{13}C {^{1}H} NMR (400 MHz, CD_3CN) δ:166.58, 165.90, 165.79, 159.63, 154.78, 154.24, 153.78, 151.35, 149.95, 149.79, 148.16, 148.47, 139.91, 139.33, 139.31, 132.14, 131.90, 130.94, 129.69, 126.13, 124.90, 124.84, 124.79, 124.77, 124.66, 124.58, 121.62, 121.31, 118.27.

MS (ESI) calcd for $[C_{34}H_{23}IrN_5O_6]^+$ 790.17, found 790.1271 (M^+).

Synthesis of $[Ir(pyba)_2$(4',4-dinitro-2,2'-bipyridine)$]PF_6$ (AS13)

The synthetic procedure was the same as that for **AS9**, except that 4',4-dinitro-2,2'-bipyridine (0.039 g, 0.16 mmol), which replaced 2,2'-bipyridine, was used. The resulting product was purified and precipitated as for **AS9**, yielding a dark red powder (40.3 mg, yield 25%)

^{1}H NMR (400 MHz, CD_3CN) δ:9.43 (s 2H, Bpy-*H*); 8.34 (d, ^3J = 6.03, 2H, Bpy-*H*); 8.23 (d, ^3J = 8.03, 2H, Pyba-*H*); 8.18 (dd, ^3J = 6.03, ^4J = 1.67, 2H, Bpy-*H*); 8.00 (t; ^3J = 8.03, 2H, Pyba-*H*); 7.98-7.95 (m, 2H, Pyba-*H*); 7.73 (d, ^3J = 8.03, 2H, Pyba-*H*); 7.67 (d, ^3J = 5.36, 2H, Pyba-*H*); 7.18 (t, ^3J = 6.19, 2H, Pyba-*H*); 6.85 (s, 2H, Pyba-*H*).

[Low solubility] ^{13}C {^{1}H} NMR (400 MHz, CD_3CN) δ:165.63, 157.76, 157.51, 155.05, 154.17, 154.13, 150.07, 150.04, 139.62, 139.22, 131.92, 131.12, 124.94, 124.92, 122.78, 121.48, 119.56.

MS (ESI) *m/z* calcd for $[C_{34}H_{22}IrN_6O_8]^+$ 835.1128, found 835.1135 (M^+).

Synthesis of [Ir(pyba)$_2$(N,N'-bis(4-methoxyphenylimino)acenaphthene)]PF$_6$ (AS14)

The synthetic procedure was the same as that for **AS9**, except that 4-MeOPh-BIAN (0.063 g, 0.16mmol), which replaced 2,2'-bipyridine, was used. The resulting product was purified and precipitated as for **AS9**, yielding a brown powder. (35 mg, yield 21%)

^{1}H NMR (400 MHz, CD_3CN) δ: 8.84 (d, ^{3}J = 5.12 Hz, 2H, Pyba -*H*); 8.31 (d, ^{3}J = 8.28 Hz, 2H, BIAN-*H*); 8.07-8.01 (m, 4H, Pyba -*H*); 7.60 (t, ^{3}J = 7.84 Hz, 2H, BIAN-*H*); 7.52 (d, ^{3}J = 7.68 Hz, 2H, Pyba-*H*); 7.47-7.41 (m, 4H, Pyba-*H*); 7.35 (d, ^{3}J = 7.56 Hz, 2H, BIAN-*H*); 6.99 (bs, 2H, BIAN-*H*); 6.73 (s, 2H, Pyba-*H*); 6.63 (bs, 4H, BIAN-*H*); 6.11 (bs, 2H, BIAN-*H*); 3.74 (s, 6H, BIAN-C*H*$_3$).

^{13}C {^{1}H} NMR (400 MHz, CD_3CN) δ:173.23, 165.73, 159.33, 151.64, 148.12, 147.63, 139.34, 137.77, 131.92, 131.54, 131.28, 130.27, 128.92, 127.27, 125.12, 124.06, 123.84, 123.80, 120.66, 114.69, 55.34.

MS (ESI) *m/z* calcd for $[C_{50}H_{34}IrN_4O_6]^+$ 981.2264, found 981.2380 (M^+).

Synthesis of [Ir(pyba)$_2$(N,N'-bis(phenylimino)acenaphthene)]PF$_6$ (AS15)

The synthetic procedure was the same as that for **AS9**, except that Ph-BIAN (0.054 g, 0.16mmol), which replaced 2,2'-bipyridine, was used. The resulting product was purified and precipitated as for **AS9**, yielding a dark green powder. (35 mg, yield 21%)

^{1}H NMR (400 MHz, DMSO-d_6) δ:9.06 (d, ^{3}J = 5.49, 2H, Pyba-*H*); 8.40 (d, ^{3}J = 8.30, 2H, BIAN-*H*); 8.24 (d, ^{3}J = 7.60, 2H, Pyba-*H*); 8.18 (d, ^{3}J = 7.04, 2H, Pyba-*H*); 7.71-7.64 (m, 2H, BIAN-*H*); 7.63-7.53 (m, 4H, Pyba-*H*); 7.30-7.18 (m, 8H, Pyba-*H*&BIAN-*H*); 7.15-7.08 (m, 2H, BIAN-*H*); 7.03-6.95 (m, 2H, BIAN-*H*); 6.53 (d, ^{3}J = 6.25, 2H, Pyba-*H*); 6.05-5.93 (m, 2H, BIAN-*H*).

[Low solubility] ^{13}C {^{1}H} NMR not recorded

HRMS (ESI) *m/z* calcd for $[C_{48}H_{32}IrN_4O_4]^+$ 921.2052, found 921.2204 (M^+)

Notes and reference

1. F. Odobel, L. Le Pleux, Y. Pellegrin and E. Blart, *Acc. Chem. Res.*, 2010, **43**, 1063-1071.
2. Y. Sun, A. C. Onicha, M. Myahkostupov and F. N. Castellano, *ACS Appl. Mater. Interfaces*, 2010, **2**, 2039-2045.
3. S. M. Zakeeruddin, M. K. Nazeeruddin, R. Humphry-Baker, P. Péchy, P. Quagliotto, C. Barolo, G. Viscardi and M. Grätzel, *Langmuir*, 2002, **18**, 952.
4. R. Jose, A. Kumar, V. Thavasi, K. Fujihara, S. Uchida and S. Ramakrishna, *Appl. Phys. Lett.*, 2008, **93**, 023125-023125-023123.
5. L. Gundlach, R. Ernstorfer and F. Willig, *Prog. Surf. Sci.*, 2007, **82**, 355-377.
6. A. Morandeira, G. Boschloo, A. Hagfeldt and L. Hammarström, *J. Phys. Chem. B*, 2005, **109**, 19403.
7. G. H. Summers, J.-F. Lefebvre, F. A. Black, E. Stephen Davies, E. A. Gibson, T. Pullerits, C. J. Wood and K. Zidek, *Phys. Chem. Chem. Phys.*, 2016, **18**, 1059.
8. C. J. Wood, K. C. D. Robson, P. I. P. Elliott, C. P. Berlinguette and E. A. Gibson, *RSC Adv.*, 2014, **4**, 5782-5791.
9. A. Morandeira, G. Boschloo, A. Hagfeldt and L. Hammarström, *J. Phys. Chem. C*, 2008, **112**, 9530.
10. E. A. Gibson, A. L. Smeigh, L. L. Pleux, J. Fortage, G. Boschloo, E. Blart, Y. Pellegrin, F. Odobel, A. Hagfeldt and L. Hammarström, *Angew. Chem. Int. Ed.*, 2009, **48**, 4402.
11. A. Nattestad, A. J. Mozer, M. K. R. Fischer, Y.-B. Cheng, A. Mishra, P. Bäuerle and U. Bach, *Nature Mat.*, 2010, **9**, 31.
12. P. Qin, J. Wiberg, E. A. Gibson, M. Linder, L. Li, T. Brinck, A. Hagfeldt, B. Albinsson and L. Sun, *J. Phys. Chem. C*, 2010, **114**, 4738.
13. J. He, H. Lindström, A. Hagfeldt and S.-E. Lindquist, *J. Phys. Chem. B*, 1999, **103**, 8940.
14. H. Zhu, A. Hagfeldt and G. Boschloo, *J. Phys. Chem. C*, 2007, **111**, 17455.
15. S. A. Sapp, C. M. Elliott, C. Contado, S. Caramori and C. A. Bignozzi, *J. Am. Chem. Soc.*, 2002, **124**, 11215.
16. A. Yella, H. W. Lee, H. N. Tsao, C. Yi, A. K. Chandiran, M. K. Nazeeruddin, E. W. Diau, C. Y. Yeh, S. M. Zakeeruddin and M. Gratzel, *Science*, 2011, **334**, 629.
17. E. A. Gibson, A. L. Smeigh, L. c. Le Pleux, L. Hammarström, F. Odobel, G. Boschloo and A. Hagfeldt, *J. Phys. Chem. C*, 2011, **115**, 9772.
18. Y. Ohsawa, S. Sprouse, K. A. King, M. K. D. Armond, K. W. Hanck and R. J. Watts, *J. Phys. Chem.*, 1987, **91**, 1047.
19. F. O. Garces, K. A. King and R. J. Watts, *Inorg. Chem.*, 1988, **27**, 3464.
20. F. Xu, H. U. Kim, J.-H. Kim, B. J. Jung, A. C. Grimsdale and D.-H. Hwang, *Prog. Pol. Sci.*, 2015, **47**, 92.
21. J. Tang, *Front. Optoelectr.*, 2015, **8**, 239.
22. K. Hasan, A. K. Bansal, I. D. Samuel, C. Roldan-Carmona, H. J. Bolink and E. Zysman-Colman, *Sci. Rep.*, 2015, **5**, 12325.
23. P. Tao, W.-L. Li, J. Zhang, S. Guo, Q. Zhao, H. Wang, B. Wei, S.-J. Liu, X.-H. Zhou, Q. Yu, B.-S. Xu and W. Huang, *Advanced Functional Materials*, 2016, **26**, 881-894.
24. W. Lin, Q. Zhao, H. Sun, K. Y. Zhang, H. Yang, Q. Yu, X. Zhou, S. Guo, S. Liu and W. Huang, *Advanced Optical Materials*, 2015, **3**, 368-375.
25. H. Sun, S. Liu, W. Lin, K. Y. Zhang, W. Lv, X. Huang, F. Huo, H. Yang, G. Jenkins, Q. Zhao and W. Huang, *Nat Commun*, 2014, **5**, 3601.
26. L. He, Y. Li, C.-P. Tan, R.-R. Ye, M.-H. Chen, J.-J. Cao, L.-N. Ji and Z.-W. Mao, *Chemical Science*, 2015, **6**, 5409-5418.
27. D.-L. Ma, L.-J. Liu, K.-H. Leung, Y.-T. Chen, H.-J. Zhong, D. S.-H. Chan, H.-M. D. Wang and C.-H. Leung, *Angewandte Chemie International Edition*, 2014, **53**, 9178-9182.
28. K. Deo, B. Pages, D. Ang, C. Gordon and J. Aldrich-Wright, *Int J Mol Sci*, 2016, **17**, 1818.
29. E. I. Mayo, K. Kilsa, T. Tirrell, P. I. Djurovich, A. Tamayo, M. E. Thompson, N. S. Lewis and H. B. Gray, *Photochem. Photobiol. Sci.*, 2006, **5**, 871-873.
30. M. Gennari, F. Légalité, L. Zhang, Y. Pellegrin, E. Blart, J. Fortage, A. M. Brown, A. Deronzier, M.-N. Collomb, M. Boujtita, D. Jacquemin, L. Hammarström and F. Odobel, *J. Phys. Chem. Lett.*, 2014, **5**, 2254-2258.
31. A. Sinopoli, C. J. Wood, E. A. Gibson and P. I. P. Elliott, *Eur. J. Inorg. Chem.*, 2016, 2887-2890.
32. J. Massin, S. Lyu, M. Pavone, A. B. Munoz-Garcia, B. Kauffmann, T. Toupance, M. Chavarot-Kerlidou, V. Artero and C. Olivier, *Dalton Trans.*, 2016, **45**, 12539-12547.
33. K. Chen, J. W. Bats and M. Schmittel, *Inorg. Chem.*, 2013, **52**, 12863-12865.
34. J. Ohata, F. Vohidov, A. Aliyan, K. Huang, A. A. Marti and Z. T. Ball, *Chem. Comm.* , 2015, **51**, 15192-15195.

35. Z. Xie, L. Ma, K. E. deKrafft, A. Jin and W. Lin, *J. Am. Chem. Soc.*, 2010, **132**, 922-923.
36. Y. Sun, S. N. Collins, L. E. Joyce and C. Turro, *Inorg. Chem.*, 2010, **49**, 4257.
37. K. R. Schwartz, R. Chitta, J. N. Bohnsack, D. J. Ceckanowicz, P. Miro, C. J. Cramer and K. R. Mann, *Inorg. Chem.*, 2012, **51**, 5082-5094.
38. K. Hasan and E. Zysman-Colman, *Eur. J. Inorg. Chem.*, 2013, **2013**, 4421.
39. C. Dragonetti, A. Valore, A. Colombo, S. Righetto and V. Trifiletti, *Inorg. Chim. Acta*, 2012, **388**, 163.
40. A. B. Tamayo, S. Garon, T. Sajoto, P. I. Djurovich, I. M. Tsyba, R. Bau and M. E. Thompson, *Inorg. Chem.*, 2005, **44**, 8723.
41. S. Lamansky, P. Djurovich, D. Murphy, F. Abdel-Razzaq, H-E Lee, C. Adachi, P. E. Burrows, S. R. Forrest and M. E. Thompson, *J. Am. Chem. Soc.*, 2001, **123**, 4304.
42. C.-H. Yang, S.-W. Li, Y. Chi, Y.-M. Cheng, Y.-S. Yeh, P.-T. Chou, G.-H. Lee, C.-H. Wang and C.-F. Shu, *Inorg. Chem.*, 2005, **44**, 7770.
43. C. E. Welby, L. Gilmartin, R. R. Marriott, A. Zahid, C. R. Rice, E. A. Gibson and P. I. P. Elliott, *Dalton Trans.*, 2013, **42**, 13527.
44. K. Hasan and E. Zysman-Colman, *Inorg. Chem.*, 2012, **51**, 12560.
45. E. A. Gibson, L. Le Pleux, J. Fortage, Y. Pellegrin, E. Blart, F. Odobel, A. Hagfeldt and G. Boschloo, *Langmuir*, 2012, **28**, 6485.
46. E. Amouyal, A. Homsi, J.-C. Chambron and J.-P. Sauvage, *Dalton Trans.*, 1990, 1841.
47. D. Wenkert and R. B. Woodward, *J. Org. Chem.*, 1983, **48**, 283.
48. G. Maerker, *J. Am. Chem. Soc.*, 1958, **80**, 2745.
49. K. Hasan and E. Zysman-Colman, *European Journal of Inorganic Chemistry*, 2013, **2013**, 4421-4429.
50. C. J. Wood, M. Cheng, C. A. Clark, R. Horvath, I. P. Clark, M. L. Hamilton, M. Towrie, M. W. George, L. Sun, X. Yang and E. A. Gibson, *J. Phys. Chem. C*, 2014, **118**, 16536.
51. M. Valiev, E. J. Bylaska, N. Govind, K. Kowalski, T. P. Straatsma, H. J. J. V. Dam, D. Wang, J. Nieplocha, E. Apra, T. L. Windus and W. d. Jong, *Comp. Phys. Commun.*, 2010, **181**, 1477-1660.
52. P. J. Stephens, F. J. Devlin, C. F. Chabalowski and M. J. Frisch, *J. Phys. Chem.*, 1994, **98**, 11623-11627.
53. D. Andrae, U. Haussermann, M. Dolg, H. Stoll and H. Preuss, *Theor. Chim. Acta*, 1990, **77**, 123-141.
54. R. Krishnan, J. S. Binkley, R. Seeger and J. A. Pople, *J. Chem. Phys.*, 1980, **72**, 650-654.
55. A. Klamt, *WIREs Comput. Mol. Sci.*, 2011, **1**, 699-709.
56. A. R.Oki and R. J. Morgan, *Synt. Commun.*, 1995, **25**, 4093.